Available online at www.sciencedirect.com
ScienceDirect
Solid State Ionics 178 (2007) 1163–1167
SOLID STATE IONICS
www.elsevier.com/locate/ssi

Crystal structure of a superionic conductor, $Li_7P_3S_{11}$

Hisanori Yamane [a,*], Masatoshi Shibata [b], Yukio Shimane [b], Tadanori Junke [b], Yoshikatsu Seino [b], Stefan Adams [c], Keiichi Minami [d], Akitoshi Hayashi [d], Masahiro Tatsumisago [d]

[a] Institute of Multidisciplinary Research for Advanced Materials, Tohoku University, 2-1-1 Katahira, Aoba-ku, Sendai 980-8577, Japan
[b] Functional Materials Laboratory, Central Research Laboratories, Idemitsu Kosan Co., Ltd. 1280 Kami-Izumi, Sodegaura, Chiba 299-0293, Japan
[c] Department of Materials Science and Engineering, Faculty of Engineering, National University of Singapore, 7 Engineering Drive 1, 117574 Singapore
[d] Department of Applied Chemistry, Osaka Prefecture University, 1-1 Gakuen-cho, Sakai, Osaka 599-8531, Japan

Received 26 March 2007; received in revised form 25 May 2007; accepted 29 May 2007

Abstract

A synchrotron X-ray powder diffraction pattern was measured for a lithium superionic conductor, $Li_7P_3S_{11}$, which has a high conductivity of 3.2×10^{-3} S cm^{-1} at room temperature and a low activation energy of 12 kJ mol^{-1} [Mizuno et al., Solid State Ionics, vol. 177 (2006) 2721]. The crystal structure was solved by a direct space global optimization technique and refined by the Rietveld method. The compound crystallizes in a triclinic cell, space group P-1, $a=12.5009(3)$ Å, $b=6.03160(17)$ Å, $c=12.5303(3)$ Å, $\alpha=102.845(3)°$, $\beta=113.2024(18)°$, $\gamma=74.467(3)°$. PS_4 tetrahedra and P_2S_7 ditetrahedra are contained in the structure and Li ions are situated between them.

Keywords: Lithium ion conductor; Lithium phosphorous sulfide; Glass ceramics; Crystal structure

1. Introduction

Sulfide-based materials, as well as other compounds with high lithium ion conductivity, have been investigated for application as a non-flammable electrolyte in solid state lithium batteries. [1–4]. Recently, super lithium ion conduction of $70Li_2S–30P_2S_5$ (mol%) glass ceramics has been discovered [5–8]. A remarkably high lithium conductivity of 3.2×10^{-3} S cm^{-1} was reported for this glass ceramics at room temperature with an extremely low activation energy of 12 kJ mol^{-1} for conduction [8].

Amorphous materials prepared by ball milling crystallize at 513–633 K to be glass ceramics. The X-ray powder diffraction pattern of the glass ceramics could not be explained based on the known crystalline phases, Li_3PS_4, $Li_4P_2S_6$ and Li_7PS_6, in the $Li_2S–P_2S_5$ system [2,9,10] nor on a series of thio-LISICONs in the $Li_2S–P_2S_5$ [5,8] and $Li_2GeS_4–Li_3PS_4$ [3,4] systems. At 823 K the new crystalline phase of the glass ceramics decomposes into $Li_4P_2S_6$ and Li_3PS_4 or a phase analogous to thio-LISICON III in the $Li_4GeS_4–Li_3PS_4$ system [6]. A mixture of $Li_4P_2S_6$ and Li_3PS_4 was obtained by solid state reaction of 70 mol% Li_2S and 30 mol% P_2S_5 at 973 K. The new crystalline phase of the glass ceramics has been regarded as being metastable.

The local structure of the new phase was investigated by Raman spectroscopy [7,8], indicating that structural units of pyro-thiophosphate ($P_2S_7^{4-}$) and ortho-thiophosphate (PS_4^{3-}) are contained in the structure. However, the crystal system and structure of the new phase were not clarified. The present paper reports the crystal structure of the new phase, $Li_7P_3S_{11}$, of the glass ceramics by using synchrotron X-ray powder diffraction data. The structure is discussed in comparison with that of a Ag-ion conductor, $Ag_7P_3S_{11}$, which also contains $P_2S_7^{4-}$ and PS_4^{3-}.

2. Experimental

$Li_2S–P_2S_5$ glass ceramics, $Li_7P_3S_{11}$ was prepared by mechanical milling and subsequent heat treatment [5–8]. A mixture of 70 mol% Li_2S (Idemitsu Kosan Co., 99.9%) and 30 mol% P_2S_5 (Aldrich, 99%) was placed in an Al_2O_3 pot with Al_2O_3 balls, and mechanically milled with a planetary ball mill apparatus (Fritsch

* Corresponding author. Tel./fax: +81 22 217 5813.
E-mail address: yamane@tagen.tohoku.ac.jp (H. Yamane).

0167-2738/$ - see front matter © 2007 Elsevier B.V. All rights reserved.
doi:10.1016/j.ssi.2007.05.020

Table 1
Crystal data and structure refinement for $Li_7P_3S_{11}$

Formula	$Li_7P_3S_{11}$	Lattice volume (Å^3)	829.35(4)
Formula weight	988.45	Density (calc.)	1.98 Mg/m^3
Crystal system	triclinic	Density (meas.)	1.91 Mg/m^3
Space group	*P*-1(No. 2)		
Z	2	X-ray wavelength (Å)	1.49738
Cell parameters		Step size (°)	0.01
a (Å)	12.5009(3)	Reliability factors	
b (Å)	6.03160(17)	R_{wp}=2.92%	R_p=2.20%
c (Å)	12.5303(3)	R_R=7.69%	R_e=1.82%
α (°)	102.845(3)	Goodness-of-fit	*S*=1.598
β (°)	113.2024(18)	R_I=1.95%	R_F=0.73%
γ (°)	74.467(3)		

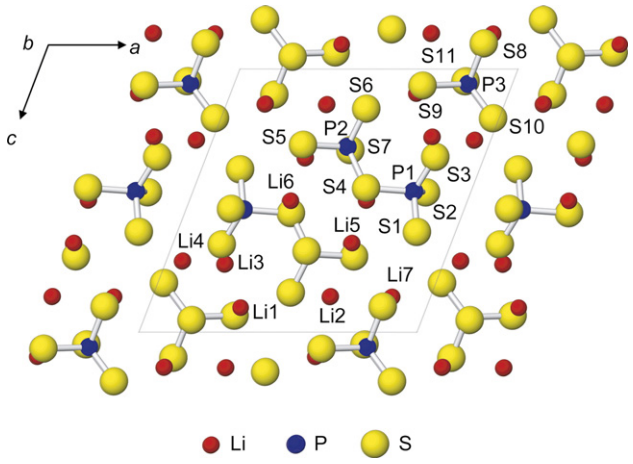

Fig. 2. Structure of $Li_7P_3S_{11}$ viewed along the [010] direction.

Pulverisette 7) for 40 h under a rotating speed of 500 rpm. Since the starting and resultant materials were hygroscopic and air-sensitive, all the processes were performed in a dry Ar-filled glove box ([H_2O] below 1 ppm).

The milled powder was placed in a stainless steel tube, which was sealed under Ar atmosphere. The sealed tube was then heated at 573 K for 2 h, followed by cooling to room temperature. The density of the obtained sample (1.91 g/cm^3) was measured by Archimedes' method with tetralin which was dehydrated with a molecular sieve before use. The sample was sealed in a boro-silicate glass capillary (I.D. ca. 0.5 mm) with Ar gas for X-ray diffraction measurement.

Synchrotron X-ray powder diffraction was carried out at 298 K using a Debye–Scherrer camera (camera length, 286.5 mm) with an imaging plate at the beam-line BL19B2 in SPring-8. The diffraction data were collected with a 0.01° step width from 6.0° to 70.0° in 2θ. The wavelength of the incident beam was calibrated with NIST SRM Ceria 640b CeO_2 powder (*a*=5.41129 Å at 298.15 K) and fixed at 1.49738 Å.

We attempted to index the diffraction peaks with a monoclinic cell and refine the structure in accordance with the structure model of $Ag_7P_3S_{11}$ (monoclinic *a*=23.97(1), *b*=6.361(4), *c*=24.88(1) Å, β=110.85(5)°, space group *C*2/*c*) [11] due to the similarity of the powder diffraction patterns of $Li_7P_3S_{11}$ and $Ag_7P_3S_{11}$. However, some major peaks in the diffraction pattern could not be indexed and the structure could not be refined with reasonable S–P–S bond angles in $P_2S_7^{4-}$ and PS_4^{3-}. The X-ray powder diffraction pattern was indexed by the triclinic cell listed in Table 1 using the JADE program [12]. The cell volume of the triclinic cell was about 1/4 of the volume of the $Ag_7P_3S_{11}$ monoclinic cell.

The structure was solved in space group *P*-1 by global optimization of a structural model in direct space using the program FOX [13]. The RIETAN2000 program [14] was used in the Rietveld analysis of the X-ray powder diffraction pattern. Three PS_4 tetrahedra with an expected P–S bond length of 2.0 Å in the asymmetric unit were set as building blocks in the starting configuration. Two of the three tetrahedra automatically shared

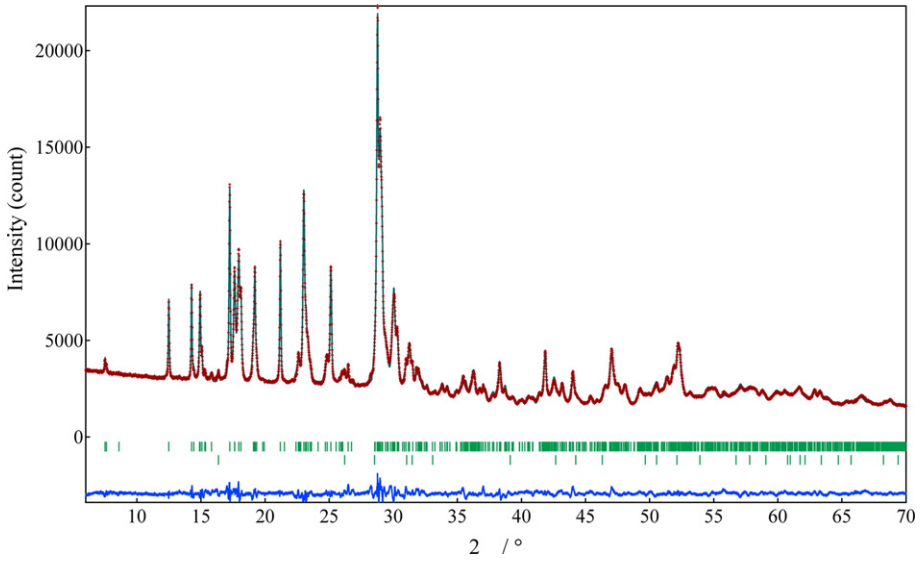

Fig. 1. Observed (dots), calculated (line) and difference (bottom line) synchrotron X-ray powder diffraction patterns (wavelength: 1.49738 Å). Vertical bars indicate the Bragg positions of contributing phases: $Li_7P_2S_{11}$ (ca. 98.5 mass%) and $Li_4P_2S_6$ (ca. 1.5 mass%).

Table 2
Atomic coordinates for $Li_7P_3S_{11}$

	x	y	z
P1	0.7938(5)	0.0334(9)	0.4654(5)
P2	0.4929(4)	0.0380(8)	0.2966(4)
P3	0.8400(6)	0.2698(10)	0.0585(6)
S1	0.8606(6)	0.2363(9)	0.6195(5)
S2	0.8235(6)	0.1052(12)	0.3342(5)
S3	0.8400(5)	−0.3171(8)	0.4680(5)
S4	0.6176(4)	0.1597(10)	0.4529(5)
S5	0.3306(5)	0.2267(10)	0.2884(6)
S6	0.5086(6)	0.0795(12)	0.1507(5)
S7	0.5094(6)	−0.2999(9)	0.3074(5)
S8	0.8406(6)	0.3302(11)	−0.0967(5)
S9	0.8279(6)	−0.0734(13)	0.0462(6)
S10	0.6781(5)	0.4874(11)	0.0640(6)
S11	0.9772(6)	0.3509(13)	0.1876(5)
Li1	0.669(2)	0.1322(19)	0.092(3)
Li2	0.6381(7)	0.402(4)	0.8657(14)
Li3	0.216(3)	0.530(7)	0.740(3)
Li4	−0.0580(10)	0.786(7)	0.270(3)
Li5	0.359(16)	0.5909(17)	0.3368(18)
Li6	0.637(3)	0.734(7)	0.498(3)
Li7	0.139(2)	0.294(6)	0.134(3)

Overall equivalent isotropic atomic displacement parameter, B=1.46(6) $Å^{-2}$.

one S atom and formed the P_2S_7 group by the program's dynamic occupancy correction during the optimization. The atomic coordinates of P_2S_7 and PS_4 given by FOX were taken as the starting model of Rietveld refinement. The positions of Li atoms were located by trial and error.

Very small peaks from trace impurities were seen in the diffraction pattern. Peaks explained by the structure of $Li_4P_2S_6$ were included in the Rietveld refinement. Other tiny peaks were not excluded in the refinement. Conventional agreement factors R_{wp}=4.88% and R_p=3.35% were obtained by the refinement. Even in the high-resolution synchrotron X-ray powder diffraction pattern, the diffraction peaks of $Li_7P_3S_{11}$ were broad. For examples, the full widths at half maximum (FWHMs) of the peaks at around 2θ=27° were 0.19°, which was almost three times wider than the FWHM (0.07°) of the CeO_2 standard 111 diffraction peak. We also observed that the widths of some peaks were obviously broader or sharper than others, in particular, $h0l$ reflection peaks were sharper. Thus, secondary profile parameters were adopted for some reflections. Final Rietveld refinement with restraints on some bond distances resulted in R_{wp}=2.92%, R_p=2.20%, and goodness-of-fit S=1.598. X-ray absorption correction was not performed in the structure refinement. The overall equivalent isotropic atomic displacement parameter B was refined to be 1.46(6) $Å^{-2}$.

A graphical comparison between the observed and calculated powder patterns is given in Fig. 1. A projection of the whole structure of $Li_7P_3S_{11}$ (drawn with ATOMS [15]) is shown in Fig. 2. The refined cell parameters and coordinates of $Li_7P_3S_{11}$ are listed in Tables 1 and 2, respectively. As shown in Fig. 1, the calculated density of $Li_7P_3S_{11}$ agreed well with the observed one. Atomic coordinates of $Li_4P_2S_6$ were fixed at the reported values [10], giving R-indexes of $Li_4P_2S_6$ R_I=2.65% and R_F=1.12%. The amount of $Li_4P_2S_6$ evaluated by the scale factors was approximately 1.5 mass%. The refined lattice parameters of $Li_4P_2S_6$ (hexagonal, space group $P6_3/mmc$) were a=6.0752(9) and c=6.6061(13) Å, which were comparable to those reported by Mercier et al. (a=6.070(4) and c=6.577(4) Å) [10].

3. Results and discussion

The $Li_7P_3S_{11}$ glass ceramics crystallizes in the triclinic centrosymmetric space group P-1 with two formula units per unit cell. All atoms in the structure are at general positions. Corner-sharing $P_2S_7^{4-}$ ditetrahedra (pyro-thiophosphate) and PS_4^{3-} tetrahedra (ortho-thiophosphate) are surrounded by Li^+ cations.

The structures of $Li_7P_3S_{11}$ and α-$Ag_7P_3S_{11}$ [16] are compared in Fig. 3. Brinkmann et al. reported that α-$Ag_7P_3S_{11}$ is a low temperature phase stable below 130 K and that seven silver atom sites in the structure are fully occupied [16]. The α-phase as well as the room-temperature phase γ-$Ag_7P_3S_{11}$ crystallize in a monoclinic cell with the space group $C2/c$. β-$Ag_7P_3S_{11}$ (130–205 K) has also been reported but the structure of this phase has not been clarified. Structural relationship

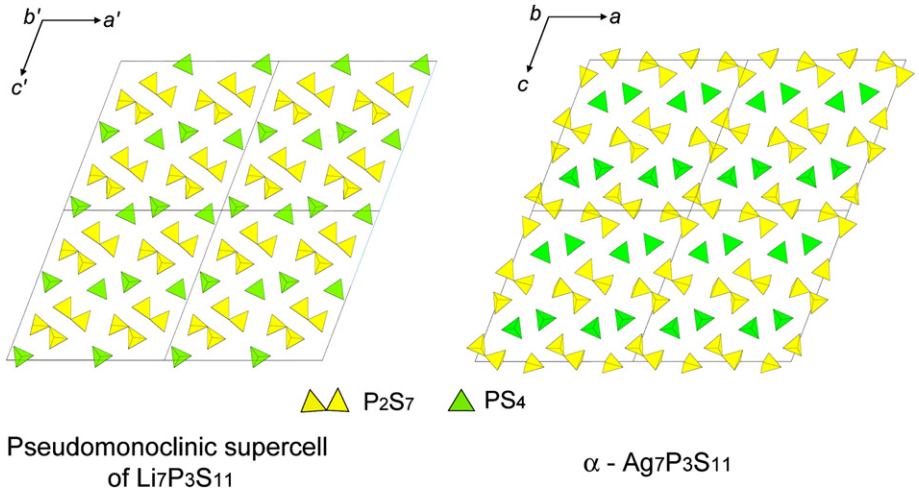

Fig. 3. Structures of $Li_7P_3S_{11}$ illustrated with the pseudomonoclinic supercell (left) and $Ag_7P_3S_{11}$ (right) viewed along the [010] direction.

between $Li_7P_3S_{11}$ becomes most obvious in a pseudo-monoclinic supercell $a'=2a-b$; $b'=b$, $c'=b+2c$ of the $Li_7P_3S_{11}$ structure with the lattice constants $a'=24.098$ Å, $b'=b=6.0316$ Å; $c'=24.438$ Å; $\alpha'=88.92°$, $\beta'=110.81°$, $\gamma'=88.42°$ (Fig. 3). The volume per formula of $Li_7P_3S_{11}$ is 414 Å^3 and about 90% of the volume of $Ag_7P_3S_{11}$ (444 Å^3). The arrangement of P_2S_7 ditetrahedra and PS_4 tetrahedra of $Li_7P_3S_{11}$ is similar to that of $Ag_7P_3S_{11}$, but the two-fold, screw and *c* glide symmetries are lost in the structure of $Li_7P_3S_{11}$, due to a different relative orientation of neighbouring PS_4^{3-} anions (Figs. 3 and 4).

The P–S bond lengths and S-P–S bond angles in $P_2S_7^{4-}$ of $Li_7P_3S_{11}$ are 1.978(3)–2.091(3) Å (average 2.033 Å) and 94.3(3)–116.8(3)°, respectively (Table 3), which are in agreement with the lengths and angles reported for $P_2S_7^{4-}$ of γ-$Ag_7P_3S_{11}$ (2.004(9)–2.142(8) Å, 96.6(4)–114.7(4)°) [11]. The bond lengths (1.927(8)–2.115(8) Å, average 2.046 Å) and angles (101.3(5)–113.4(4)°) in P3–S_4 tetrahedron of $Li_7P_3S_{11}$ are also comparable with those in PS_4 of γ-$Ag_7P_3S_{11}$ (2.034(9)–2.055(9) Å, 102.3(4)–111.4(4)°) [11] and Li_3PS_4 (2.042(7)–2.068(8) Å, 106.3(2)–114.0(4)°) [9]. The bond valence sums for atoms P1, P2 and P3, calculated with the bond valence parameter of P^V–S^{II} (2.11 Å) presented by Brese and O'Keeffe [17], are close to the formal valence of P^V.

In the present study of $Li_7P_3S_{11}$, seven fully occupied lithium sites were refined as listed in Table 2. The bond valence sums for the Li sites, calculated with the bond valence parameter of Li^I–S^{II}=1.94 Å [17], were in the range 0.89–1.11, which is close to the formal valence of Li^I. However, the lithium atom positions fairly depended on the level of the restraints on Li–S bond lengths. Without these restraints, some lithium atom sites move to the positions with Li–S distances around 1.8 to 1.9 Å. In the Ag-ion conductor γ-$Ag_7P_3S_{11}$, 14 disordered silver sites were presented by Toffoli et al. [11], and 16 disordered silver positions were taken into account by Brinkmann et al. [16]. In the structure of $Li_7P_3S_{11}$, there might be some disordered lithium sites as observed in γ-$Ag_7P_3S_{11}$. In order to find such disordered (or interstitial) sites of lithium, differential Fourier synthesis was carried out with the observed *F* data extracted by Rietveld analysis. We also added 15 interstitial sites and refined the occupation factors of lithium at the Li sites and the interstitial sites. However, we could not show the presence of interstitial or disordered sites clearly. Structure analysis by high-resolution neutron powder diffraction of $Li_7P_3S_{11}$ may reveal the precise positions and diffusion paths of Li cations.

Li–S interatomic distances, calculated with the refined coordinates in Table 2, are in the range of 2.227(3)–3.09(2) Å. The Li–S distances reported for Li_3PS_4 and $Li_4P_2S_6$ are 2.41(4)–3.111(4) Å and 2.630(2) Å, respectively [9,10]. The Li–S distances of 2.369(5)–2.929(3) Å were shown by Rietveld analysis with the neutron powder diffraction data of Li_4GaS_4 [18]. Shorter Li–S distances of 2.00(5), 2.15(5) and 2.29(3) Å have been reported in the crystal structure refinement of $Li_xMo_6S_8$ (x=1, 3, 4) by neutron powder diffraction [19]. The lengths of 2.29(1)–3.04(9) Å and 2.29(7)–2.59(7) Å have also been reported for Li_2FeS_2 [20] and $LiGaS_2$ [21]. The Li1, 3, 4, 6 and 7 sites of $Li_7P_3S_{11}$ are surrounded by 4 S atoms, while on the contrary, the Li2 site and the Li5 site are surrounded by 3 and 5 S atoms, respectively.

Li–Li interatomic distances are also listed in Table 3. The shortest Li–Li interatomic distance is 2.564(4) Å, which is comparable to the shortest Li–Li distance of 2.52(10) and 2.769 Å reported for Li_3PS_4 [9] and $Li_4P_2S_6$ [10], respectively. There is a gap between the ranges from 2.564(4) to 3.93(5) Å and from 4.249(15) to 4.47(6) Å in the Li–Li distances of $Li_7P_3S_{11}$.

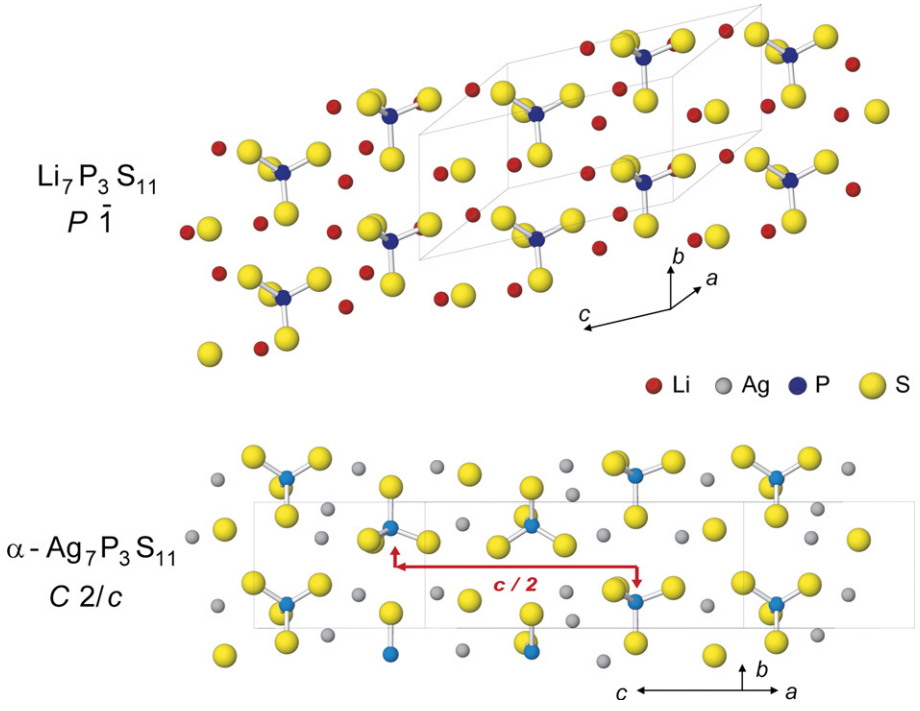

Fig. 4. Structures of $Li_7P_3S_{11}$ (*a*: 0.56–1.00) (top) and $Ag_7P_3S_{11}$ (*a*: 0.00–0.24) (bottom) viewed perpendicular to the *b*–*c* planes.

Table 3
Selected interatomic distances (Å), bond valences (*s*), and bond angles (°) in $Li_7P_3S_{11}$

P1–S2	1.978(3)	1.429	Li3–S10	2.29(4)	0.388
P1–S1	2.037(3)	1.218	Li3–S2	2.43(4)	0.266
P1–S3	2.041(3)	1.205	Li3–S3	2.55(4)	0.192
P1–S4	2.083(3)	1.076	Li3–S11	2.77(4)	0.106
		∑*s* 4.93			∑*s* 0.95
P2–S6	1.988(3)	1.391	Li4–S1	2.289(5)	0.389
P2–S5	2.019(3)	1.279	Li4–S2	2.29(4)	0.388
P2–S7	2.023(3)	1.265	Li4–S11	2.58(4)	0.177
P2–S4	2.091(3)	1.053	Li4–S9	2.80(3)	0.098
		∑*s* 4.92			∑*s* 1.05
P3–S11	1.927(8)	1.640	Li5–S5	2.227(3)	0.460
P3–S8	2.059(8)	1.148	Li5–S7	2.335(3)	0.344
P3–S9	2.083(8)	1.076	Li5–S4	2.675(16)	0.137
P3–S10	2.115(8)	0.987	Li5–S1	2.880(14)	0.079
		∑*s* 4.85	Li5–S8	3.09(2)	0.045
Li1–S9	2.256(3)	0.426			∑*s* 1.065
Li1–S10	2.288(5)	0.390	Li6–S7	2.29(4)	0.388
Li1–S6	2.500(9)	0.220	Li6–S5	2.51(4)	0.214
Li1–S2	2.89(4)	0.077	Li6–S3	2.64(4)	0.151
		∑*s* 1.11	Li6–S4	2.68(4)	0.135
Li2–S10	2.297(17)	0.381			∑*s* 0.89
Li2–S7	2.312(7)	0.366	Li7–S11	2.289(7)	0.389
Li2–S8	2.319(5)	0.359	Li7–S5	2.42(3)	0.273
		∑*s* 1.11	Li7–S9	2.48(3)	0.232
			Li7–S8	2.51(3)	0.214
					∑*s* 1.11
Li2–Li5	2.564(4)		S1–P1–S2		113.3(4)
Li1–Li3	2.81(6)		S1–P1–S3		116.8(3)
Li3–Li4	3.05(5)		S1–P1–S4		94.3(3)
Li5–Li6	3.13(4)		S2–P1–S3		108.8(4)
Li1–Li2	3.42(3)		S2–P1–S4		111.7(4)
Li5–Li6	3.49(4)		S3–P1–S4		111.2(4)
Li5–Li7	3.51(3)		S4–P2–S5		107.9(3)
Li1–Li4	3.64(3)		S4–P2–S6		115.5(4)
Li2–Li7	3.73(3)		S4–P2–S7		105.0(3)
Li4–Li7	3.86(4)		S5–P2–S6		104.2(3)
Li3–Li6	3.93(5)		S5–P2–S7		112.3(3)
Li1–Li2	4.249(15)		S6–P2–S7		112.0(4)
Li5–Li5	4.35(5)		P1–S4–P2		114.5(3)
Li2–Li7	4.37(4)		S8–P3–S9		110.1(4)
Li6–Li7	4.37(5)		S8–P3–S10		101.3(5)
Li1–Li7	4.39(3)		S8–P3–S11		110.6(4)
Li7–Li7	4.40(7)		S9–P3–S10		108.5(4)
Li1–Li1	4.47(6)		S9–P3–S11		112.4(5)
			S10–P3–S11		113.4(4)

Although the diffusion path of lithium ion could not be indicated in the present study, the fast lithium ion conduction must be realized through many interstitial sites and open space between P_2S_7 ditetrahedra and PS_4 tetrahedra in the structure of $Li_7P_3S_{11}$. The present structural results for $Li_7P_3S_{11}$ will constitute the basis for ongoing studies on the lithium conduction mechanism in $Li_7P_3S_{11}$ by computational methods including molecular dynamics simulations and dynamic bond valence analyses as well as future neutron diffraction studies.

4. Conclusions

The structure of the super lithium ion conductor, $Li_7P_3S_{11}$, was determined by using synchrotron X-ray powder diffraction data. The compound crystallizes in the triclinic cell, space group *P*-1, and contains P_2S_7 ditetrahedra and PS_4 tetrahedra similar to the case of Ag-ion conductor $Ag_7P_3S_{11}$ (monoclinic, space group *C*2/*c*). The positions of P_2S_7 ditetrahedra and PS_4 tetrahedra in the structure of $Li_7P_3S_{11}$ were determined by the direct space method and the structure was refined by the Rietveld method. Lithium ions are located at the sites around the P_2S_7 and PS_4 groups and surrounded by 3 to 5 sulfur atoms. The interstitial sites, disorder sites and diffusion paths of Li ions were not determined in the present study. Further structural studies by neutron diffraction and theoretical approaches are expected to elucidate the structural origin of the superionic conduction of $Li_7P_3S_{11}$.

Acknowledgement

The synchrotron radiation experiments were performed at the BL19B2 in the SPring-8 with the approval of the Japan Synchrotron Radiation Research Institute (JASRI) (Proposal No. 2006A0248).

References

[1] M. Tachez, J.-P. Malugani, R. Mercier, G. Robert, Solid State Ionics 14 (1984) 181.
[2] H. Eckert, Z. Zhang, J.H. Kennedy, Chem. Mater. 2 (1990) 273.
[3] R. Kanno, T. Hata, Y. Kawamoto, M. Irie, Solid State Ionics 130 (2000) 97.
[4] R. Kanno, M. Murayama, J. Electrochem. Soc. 148 (2001) A742.
[5] A. Hayashi, S. Hama, T. Minami, M. Tatsumisago, Electrochem. Commun. 5 (2003) 111.
[6] F. Mizuno, A. Hayashi, K. Tadanaga, M. Tatsumisago, Electrochem. Solid-State Lett. 8 (2005) A603.
[7] F. Mizuno, A. Hayashi, K. Tadanaga, M. Tatsumisago, Adv. Mater. 17 (2005) 918.
[8] F. Mizuno, A. Hayashi, K. Tadanaga, M. Tatsumisago, Solid State Ionics 177 (2006) 2721.
[9] R. Mercier, J.-P. Malugani, B. Fahys, G. Robert, Acta Crystallogr. B Struct. Crystallogr. Cryst. Chem. 38 (1982) 1887.
[10] R. Mercier, J.-P. Malugani, B. Fahys, J. Douglade, G. Robert, Solid State Chem. 43 (1982) 151.
[11] P. Toffoli, P. Khodadad, N. Rodier, Acta Crystallogr., B Struct. Crystallogr. Cryst. Chem. 38 (1982) 2374.
[12] JADE version 6, an XRD pattern-processing software program, Materials Data Inc., Livermore, CA.
[13] V. Favre-Nicolin, R. Cerny, J. Appl. Crystallogr. 35 (2002) 734.
[14] F. Izumi, T. Ikeda, Mater. Sci. Forum 321-324 (2000) 198.
[15] E. Dowty, ATOMS. Version 6.2. Shape Software, Kingsport, Tennessee, USA.
[16] C. Brinkmann, H. Eckert, D. Wilmer, M. Vogel, J.S. auf der Günne, W. Hoffbauer, F. Rau, A. Pfitzner, Solid State Sci. 6 (2004) 1077.
[17] N.E. Brese, M. O'Keeffe, Acta crystallogr., B Struct. Crystallogr. Cryst. Chem. 47 (1991) 192.
[18] M. Murayama, R. Kanno, Y. Kawamoto, T. Kamiyama, Solid State Ionics 154-155 (2002) 789.
[19] C. Ritter, E. Gocke, C. Fischer, R. Schöllhorn, Mater. Res. Bull. 27 (1992) 1217.
[20] L. Blandeau, G. Ouvrard, Y. Calage, R. Brec, J. Rouxel, J. Phys. C: Solid State Phys. 20 (1987) 4271.
[21] J. Leal-Gonzalez, S.S. Melibary, A.J. Smith, Acta Crystallogr., C Cryst. Struct. Commun. 46 (1990) 2017.